Progress In Electromagnetics Research M, Vol. 115, 1–10, 2023

Effect of the Temperature and the Geometrical Parameters on the Modal Properties of Circular Photonic Crystal Fiber

Mohammed Chamse Eddine Ouadah[1, 2, *], Mohammed Debbal[2, 3], Hicham Chikh-Bled[2, 4], and Mouweffeq Bouregaa[2, 5]

Abstract—This paper presents a proposal for a high birefringence photonic crystal fiber (C-PCF) with a doped liquid into two first ring holes, which is analyzed by the finite element method. It is demonstrated that the proposed fiber has a birefringence value of about 2.643×10^{-2} at wavelength $\lambda = 1.55\,\mu m$ and temperature $T = 25°C$. Also, a high chromatic dispersion of $-272\,ps/nm/km$, an effective area of $1.693\,\mu m^2$, and a confinement loss of $0.058\,dB/m$ for the x-polarization method were obtained at the same wavelength and temperature. The temperature influence on the modal properties has also been studied.

We will demonstrate through the result that the fiber we propose can be used in both sensing and chromatic dispersion applications such as flattened dispersion fibers.

1. INTRODUCTION

A new generation of optical waveguide known as a photonic crystal fiber (PCF) [1] consists of an array of air holes that appear on a background material, usually silica [2].

Mainly, the propagation of light occurs in the core of the fiber by the principle of total internal reflection, guidance due to the presence of a periodic low index air hole in the fiber cladding [3].

Therefore, photonic crystal fibers have been used in several interests [4, 5], to their ability of optical characteristics that cannot be achieved with the conventional optical fibers [6].

For example, they have been used in telecommunication sensors [7], dispersion compensating fibers [8], demultiplexers [9], filters [10], and splitters [11, 12].

To get a high birefringence, many photonic crystal fibers have been suggested. For example, Agbemabiese and Akowuah proposed a new hexagonal photonic crystal fiber (PCF) structure with four circular air hole rings [13] with a birefringence of 2.018×10^{-2} at wavelength $\lambda = 1.55\,\mu m$. On the other hand, a pentagonal PCF with an elliptical defected core (E-DC) having a birefringence value of 8×10^{-3} was proposed by Yu et al. [14].

In addition, Ahmed et al. [15] showed a square shape photonic crystal fiber (S-PCF) where three layers square cladding has enclosed the single layer core region with a high birefringence in the order of 2.2×10^{-2} at $\lambda = 1.55\,\mu m$. However, the non-circular air holes, around the solid core, cause difficulties in the fabrication process, which becomes much easier by using a drilling method [16] or a stack-and-pull technique [17], when the PCF design is limited to circular air holes [18].

In this work, we propose a circular photonic crystal fiber with two holes doped by cargille liquid [19]. We will try to have a better value of the birefringence in a wavelength of $1.55\,\mu m$ at a temperature

Received 5 November 2022, Accepted 20 December 2022, Scheduled 27 December 2022

* Corresponding author: Mohammed Chamse Eddine Ouadah (mohammedchamseeddine.ouadah@ummto.dz).

[1] Department of Telecommunications, Faculty of Electrical and Computer Engineering, Mouloud MAMMERI University, Tizi-Ouzou 15000, Algeria. [2] Telecommunications Laboratory of Tlemcen (LTT), Tlemcen 13000, Algeria. [3] Belhadj BOUCHAIB University, Ain-Temouchent 46000, Algeria. [4] Abou-Bekr BELKAID University, Tlemcen 13000, Algeria. [5] Mustapha STAMBOULI University, Mascara 29000, Algeria.

of the liquid that will be fixed ($T = 25°C$), which makes our structure a good potential candidate for high-speed broadband optical communication [20].

The second part of the work is the variation of the chromatic dispersion, low confinement loss, and the effective mode area as a function of temperature. This allows us to have a temperature sensor with the same proposed structure.

This study allowed us to open doors in the field of sensing applications [21–23].

2. MATERIAL AND DESIGNS

Figure 1 illustrates the circular photonic crystal fiber fused in silica of which two holes in the first ring are doped with liquid cargille.

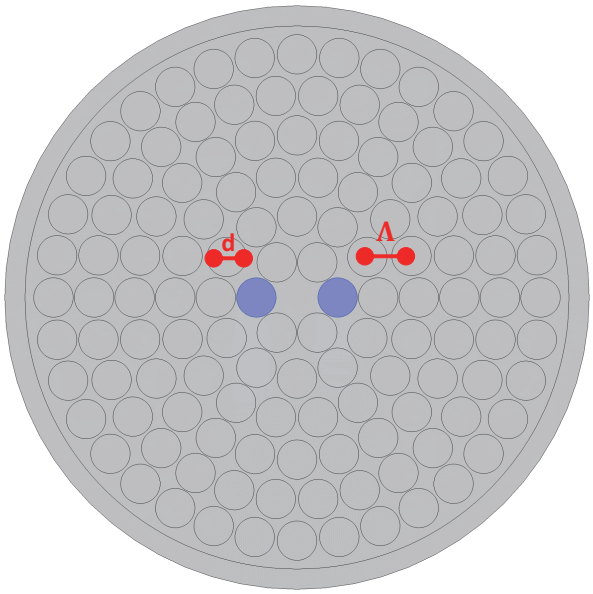

Figure 1. Circular photonic crystal fiber.

(Λ) is the parameter of the spacing between the centers of the two adjacent holes, and (d) is the diameter of the holes. The optimum geometrical parameters are presented in Table 1.

Table 1. The optimum geometrical parameters of the designed circular photonic crystal fiber.

Pitch (Λ)	Air holes diameters (d)
0.72 [µm]	0.7 [µm]

The background silica material and cargille liquid have been taken into account as presented in the following equation [24–26].

$$n^2_{Silica} = 1 + \frac{0.696166300\lambda^2}{\lambda^2 - (0.00467914826)} + \frac{0.407942600\lambda^2}{\lambda^2 - (0.0135120631)} + \frac{0.897479400\lambda^2}{\lambda^2 - 97.9340025} \quad (\lambda \text{ in } \mu\text{m}) \tag{1}$$

where n_{Silica} is the refractive index of silica, and λ is the wavelength in µm.

$$n_{Liquid}(\lambda) = 1.447925 + \frac{4073.4}{\lambda^2} + \frac{41636939}{\lambda^4} \quad (\lambda \text{ in nm}) \tag{2}$$

where $n_{Liquid}(\lambda)$ is the refractive index of liquid cargille at $T = 25°\text{C}$.

For this kind of the selected liquid infiltrated PCF, we can modify the refractive index by modifying the temperature of the infiltrating liquid, as well as adjust the modals properties according to the requirement.

Since the temperature coefficient of the liquids (α) available from M/s Cargile lab [26] is on the order of $-0.000389/°\text{C}$ in the following temperature range 15–35°C, which is much larger than that of fused silica, the smallest temperature changes will only affect the refractive index of the liquid.

The tunability of the refractive index of the liquid can be described as [26].

$$n_{Liquid\ Tunability} = n_{Liquid} + \alpha(T - 25) \tag{3}$$

T is the variable of the temperature change in °C.

Subsequently, we do a study of the geometrical parameters (Λ, d) and the temperature (T) on the properties of the proposed fiber, in order to have important optical characteristics for particular applications.

To calculate the birefringence, chromatic dispersion, and confinement loss, Comsol Multiphysics based on the finite element method with perfectly matched layers (PML) is used to solve the Maxwell's equations [27].

$$\nabla\times\left([s]^{-1}\nabla\times\vec{E}\right)k_0^2n^2[s]\vec{E}=0 \tag{4}$$

where $\vec{E}$ is the electric field vector, k_0 the free space wave number, n the refractive index of the effective medium, $[s]$ the matrix of the PML layers, and $[s]^{-1}$ the matrix inverse of $[s]$.

In our calculation we use the following equations [28].

The chromatic dispersion:

$$D = -\frac{\lambda}{c}\frac{d^2\text{Re}(n_{eff})}{d\lambda^2} \tag{5}$$

The birefringence:

$$B = |n_x - n_y| \tag{6}$$

The effective area:

$$A_{eff} = \frac{\left(\iint |E|^2\, dxdy\right)^2}{\iint |E|^4\, dxdy} \tag{7}$$

The confinement loss:

$$L_c = \frac{2\pi}{\lambda}\frac{20}{\ln(10)}10^6\text{Im}\left(n_{eff}\right) \tag{8}$$

where $\text{Re}(n_{eff})$ and $\text{Im}(n_{eff})$ are the real and imaginary parts of the effective index; λ is the wavelength; c is the velocity of light in a vacuum; n_x and n_y are the effective index of each fundamental mode.

3. RESULTS

The intensity distributions of the fundamental guided mode for x and y polarizations modes are illustrated in Figure 2.

Note that at wavelength ($\lambda = 1.55\,\mu\text{m}$), it is clear that the electric fields of the polarizations modes x and y are confined into the core fiber.

Figure 3 presents the result of the study of the chromatic dispersion as a function of the wavelength, where the temperature is fixed here at $T = 25°\text{C}$.

As shown in the present case, the negative chromatic dispersion for the y-polarization mode is larger than the x-polarization mode. The corresponding values of chromatic dispersion are $-272\,\text{ps/nm/km}$ and $-516.3\,\text{ps/nm/km}$ for x-polarization and y-polarization modes at the wavelength $\lambda = 1.55\,\mu\text{m}$.

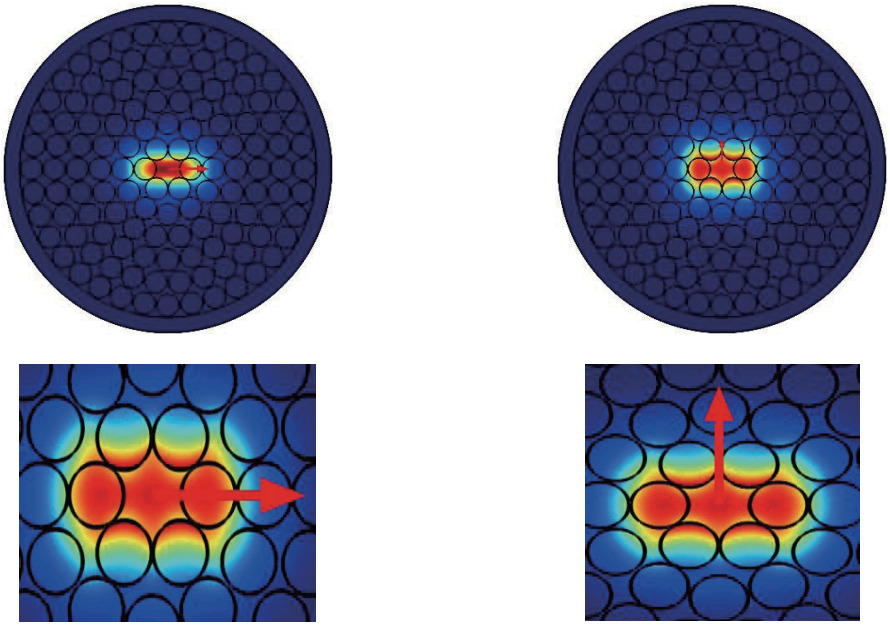

Figure 2. Electric field distribution for (a): x polarization mode, (b): y polarization mode.

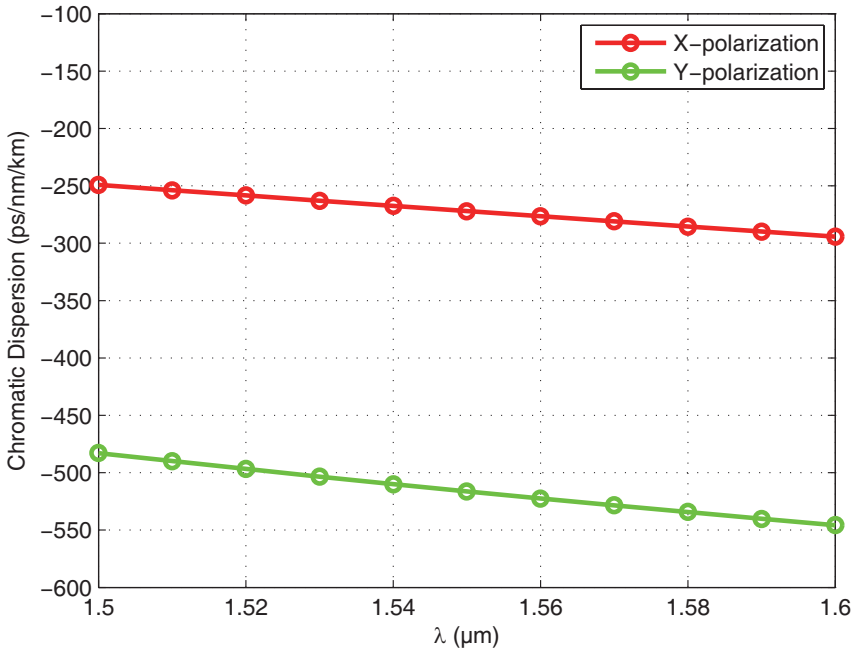

Figure 3. Chromatic dispersion curve as function of the wavelength.

Figure 4 depicts the variation of birefringence as a function of the wavelength for the optimum design parameters.

As seen in the figure above, the birefringence is 2.643×10^{-2} at the operating wavelength $\lambda = 1.55\,\mu$m, which may be used to eliminate the polarization mode dispersion in transmitting data.

In this section, we will vary the birefringence according to the opt-geometric parameters (d and Λ). Figure 5 presents the effect of the pitch (Λ) on the birefringence.

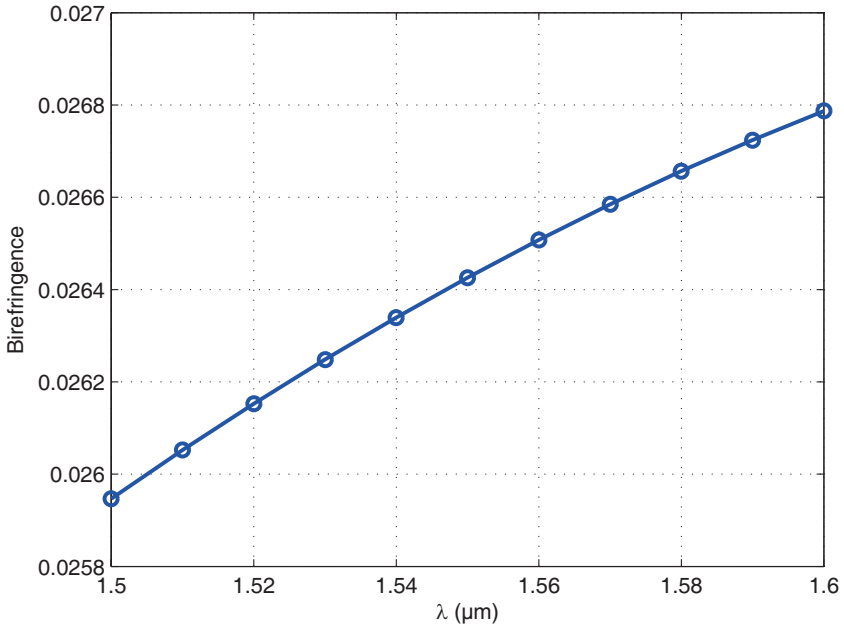

Figure 4. Birefringence as wavelength for optimum design parameters.

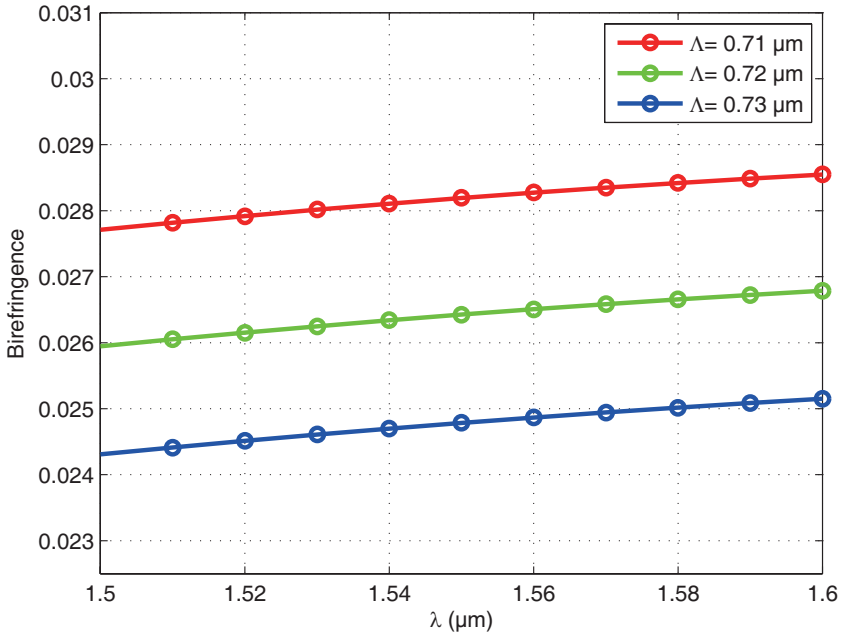

Figure 5. Effects of the pitch (Λ) on the birefringence.

It is clearly visible that there is an inverse relationship between the two parameters. As we increase the values of the pitch, the value of the birefringence decreases.

The effects of the air hole diameters (d) on the birefringence are depicted in Figure 6.

As the diameters of the air-holes increase, the birefringence increases. Moreover, the birefringence of the proposed C-PCF to the corresponding air-holes diameters $d = 0.69$, 0.7, and 0.71 µm are 2.49×10^{-2}, 2.643×10^{-2}, and 2.8×10^{-2} respectively at a wavelength of $\lambda = 1.55$ µm.

Figure 7 shows the relationship between the effective area and the wavelength for the optimum design at the temperature $T = 25°\text{C}$.

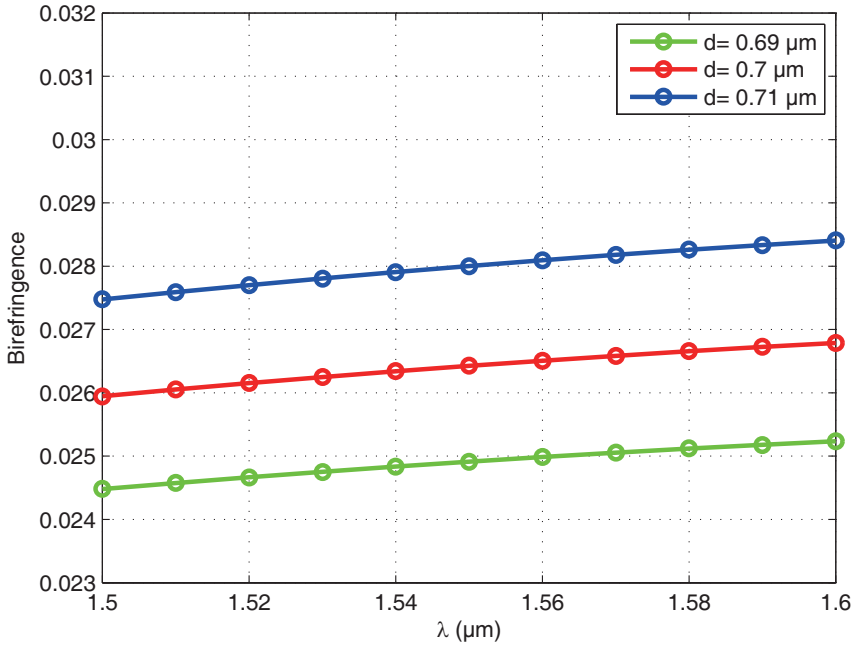

Figure 6. Effects of diameters (d) on the birefringence.

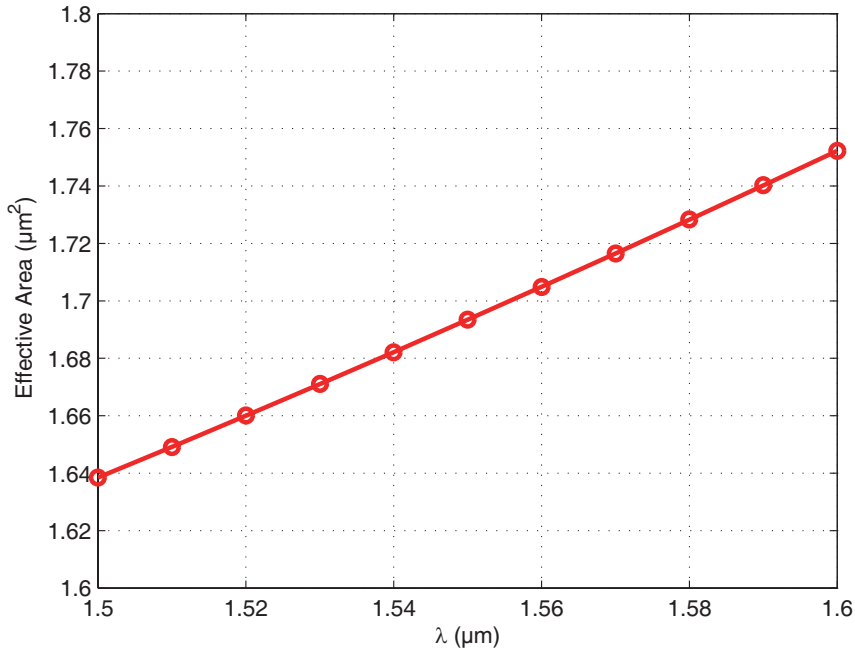

Figure 7. Effective area as wavelength for optimum design parameters.

In fact, it shows that the effective area is about $1.693\,\mu m^2$ at the operating wavelength $\lambda = 1.55\mu m$ for the x polarization mode. With this value, we can say that the proposed photonic crystal fiber can be used for some applications such as supercontinuum and soliton pulse transmission [29, 30].

Following Equation (8), Figure 8 shows the variation of the confinement loss as a function of the wavelength for the x polarization mode.

According to Figure 8, it is observed that the value of the confinement loss is about $0.058\,dB/m$ at a wavelength $\lambda = 1.55\,\mu m$. We also note that after this operating wavelength, the confinement loss

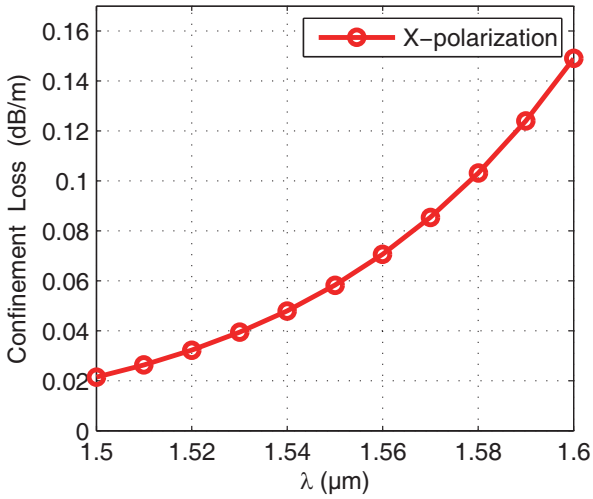

Figure 8. Confinement loss of the proposed photonic crystal fiber for x polarization mode.

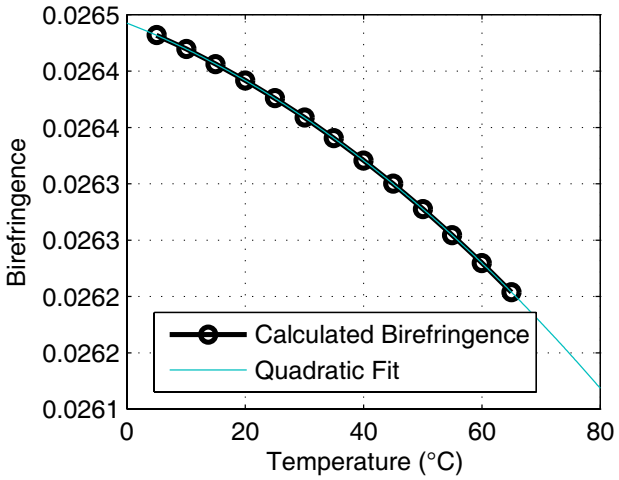

Figure 9. Impacts of the Temperature on birefringence.

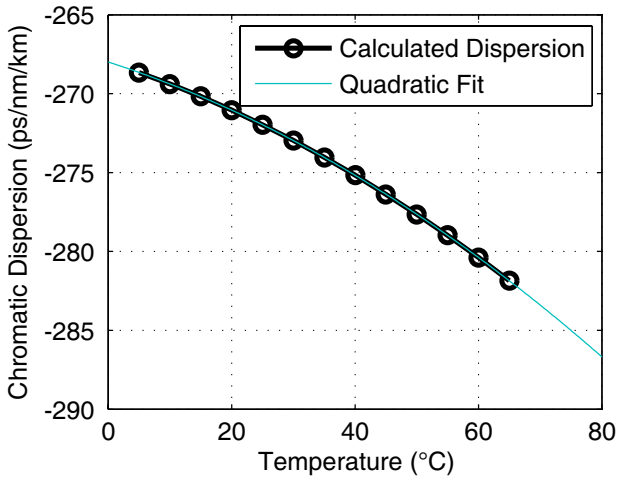

Figure 10. Impacts of the temperature on chromatic dispersion.

increases as well.

Following the various simulations with optical parameters, we have demonstrated that our fiber design is perfectly used for optical transmissions. We have achieved very good birefringence values compared to what is found in the literature.

To validate our results, a comparison is made in Table 2 between the properties of the proposed fiber and previously designs.

Table 2. Comparison between the results of the proposed fiber with others works.

	[31]	[13]	Our proposed Fiber
Birefringence	3.6×10^{-3}	2.018×10^{-2}	2.643×10^{-2}

In this second part of the paper, we will discuss the variation of the temperature with the previous parameters. The main purpose of this study is to prove that our optical fiber can react as a sensor.

Now, Figure 9 represents the variation of the birefringence with respect of the operating wavelength $\lambda = 1.55\,\mu m$ for different temperature values.

As we can see, the birefringence decreases almost linearly when the temperature rises. The effect of temperature on chromatic dispersion is also analyzed by Figure 10.

Figure 10 clearly shows that the chromatic dispersion increases with increasing temperature. Furthermore, their corresponding values are $-268.66\,ps/nm/km$, $-272\,ps/nm/km$, and $-281.85\,ps/nm/km$ for $T = 5°C$, $25°C$, and $65°C$.

Both Figure 11(a) and Figure 11(b) show the temperature effect on the effective area and the confinement loss at wavelength $\lambda = 1.55\,\mu m$.

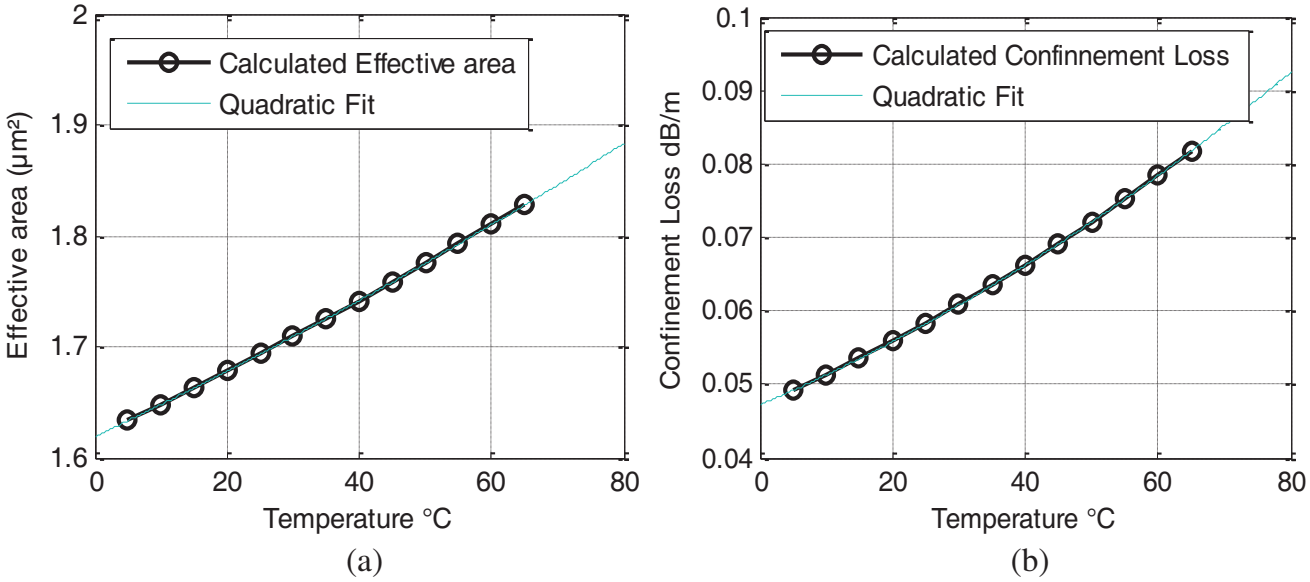

Figure 11. Impacts of temperature on effective area and the confinement loss.

From Figure 11(a), we can see that the effective area decreases with decreasing the temperature, in which the value of the effective area can be up to $1.828\,\mu m^2$ at the wavelength $\lambda = 1.55\,\mu m$ for $T = 65°C$. However, Figure 11(b) reveals that the confinement loss increases when the temperature value increases. It is observed that its value is $0.082\,dB/m$ at a wavelength $\lambda = 1.55\,\mu m$ for $T = 65°C$.

4. CONCLUSION

In this work, the modal properties of the circular photonic crystal fiber doped with the Cargile liquid have been simulated. The numerical results indicate a high birefringence of 2.643×10^{-2} at a wavelength $\lambda = 1.55\,\mu m$ and a temperature $T = 25°C$. The proposed fiber has a negative chromatic dispersion about $-272\,ps/nm/km$ at the same wavelength and temperature.

The change in temperature affects the values of the birefringence, chromatic dispersion, effective area, and confinement loss. In conclusion, the proposed photonic crystal fiber is suitable for various sensing applications, as well as other applications such as dispersion compensation.

REFERENCES

1. Knight, J. C., "Photonic crystal fibres," *Nature*, Vol. 424, No. 6950, 847–851, 2003.
2. Knight, J., T. Birks, P. S. J. Russell, and D. Atkin, "All-silica single-mode optical fiber with photonic crystal cladding," *Optics Letters*, Vol. 21, No. 19, 1547–1549, 1996.
3. Xiao, L., W. Jin, and M. Demokan, "Photonic crystal fibers confining light by both index-guiding and bandgap-guiding: hybrid PCFs," *Optics Express*, Vol. 15, No. 24, 15637–15647, 2007.

4. Zhang, L. and C. Yang, "A novel polarization splitter based on the photonic crystal fiber with nonidentical dual cores," *IEEE Photonics Technology Letters*, Vol. 16, No. 7, 1670–1672, 2004.
5. Yuan, J., G. Zhou, H. Liu, C. Xia, X. Sang, Q. Wu, C. Yu, K. Wang, B. Yan, and Y. Han, "Coherent anti-Stokes Raman scattering microscopy by dispersive wave generations in a polarization maintaining photonic crystal fiber," Vol. 141, 659–670, 2013.
6. Baggett, J. C., T. M. Monro, K. Furusawa, and D. Richardson, "Comparative study of large-mode holey and conventional fibers," *Optics Letters*, Vol. 26, No. 14, 1045–1047, 2001.
7. Podder, E., M. Hossain, R. H. Jibon, A. A.-M. Bulbul, and H. S. J. F. O. O. Mondal, "Chemical sensing through photonic crystal fiber: sulfuric acid detection," Vol. 12, No. 4, 372–381, 2019.
8. Ouadah, M. C. E. and M. E. K. Chikh-Bled, "Novel high negative chromatic dispersion photonic crystal fiber with low confinement loss," *Journal of Electrical and Electronics Engineering*, Vol. 9, No. 1, 25, 2016.
9. Dadabayev, R., N. Shabairou, Z. Zalevsky, and D. Malka, "A visible light RGB wavelength demultiplexer based on silicon-nitride multicore PCF," *Optics & Laser Technology*, Vol. 111, 411–416, 2019.
10. Rahman, Md. M., A. Khaleque, Md. T. Rahman, and F. Rabbi, "Gold-coated photonic crystal fiber based polarization filter for dual communication windows," Vol. 461, 125293, 2020.
11. An, S., J. Lv, Z. Yi, C. Liu, L. Yang, F. Wang, Q. Liu, W. Su, X. Li, T. Sun, and P. K. Chu, "Ultra-short and dual-core photonic crystal fiber polarization splitter composed of metal and gallium arsenide," Vol. 226, 165779, 2021.
12. Khan, K. R., S. Bidnyk, and T. J. Hall, "Tunable all optical switch implemented in a liquid crystal filled dual-core photonic crystal fiber," Vol. 22, 179–189, 2012.
13. Agbemabiese, P. A. and E. K. Akowuah, "Numerical analysis of photonic crystal fiber of ultra-high birefringence and high nonlinearity," *Scientific Reports*, Vol. 10, No. 1, 1–12, 2020.
14. Yu, F., Z. Wang, W. Yang, and C. Lv, "Characteristics of highly birefringent photonic crystal fiber with defected core and equilateral pentagon architecture," *Advances in Opto Electronics*, 2016.
15. Ahmed, K., B. K. Paul, Md. S. Islam, S. Chowdhury, S. Sen, Md. I. Islam, and S. Asaduzzaman, "Ultra high birefringence and lower beat length for square shape PCF: Analysis effect on rotation angle and eccentricity," *Alexandria Engineering Journal*, Vol. 57, No. 4, 3683–3691, 2018.
16. Zhang, P., J. Zhang, P. Yang, S. Dai, X. Wang, and W. Zhang, "Fabrication of chalcogenide glass photonic crystal fibers with mechanical drilling," *Optical Fiber Technology*, Vol. 26, 176–179, 2015.
17. Pysz, D., I. Kujawa, R. Stępień, M. Klimczak, A. Filipkowski, M. Franczyk, L. Kociszewski, J. Buźniak, K. Haraśny, and R. Buczyński, "Stack and draw fabrication of soft glass microstructured fiber optics," *Bulletin of the Polish Academy of Sciences. Technical Sciences*, Vol. 62, No. 4, 2014.
18. Liu, Y., X. Jing, H. Chen, J. Li, Y. Guo, S. Zhang, H. Li, and S. Li, "Highly sensitive temperature sensor based on Sagnac interferometer using photonic crystal fiber with circular layout," Vol. 314, 112236, 2020.
19. Sacher, R. and W. Sacher, "Optical liquids," *CRC Handbook of Laser Science and Technology*, 97–112, CRC Press, 2020.
20. Garlinska, M., A. Pregowska, K. Masztalerz, and M. J. F. I. Osial, "From mirrors to free-space optical communication — historical aspects in data transmission," Vol. 12, No. 11, 179, 2020.
21. Portosi, V., D. Laneve, M. C. Falconi, and F. J. S. Prudenzano, "Advances on photonic crystal fiber sensors and applications," Vol. 19, No. 8, 1892, 2019.
22. Bing, P., J. Sui, G. Wu, X. Guo, Z. Li, L. Tan, and J. Yao, "Analysis of dual-channel simultaneous detection of photonic crystal fiber sensors," Vol. 15, No. 4, 1071–1076, 2020.
23. Sultana, J., Md. S. Islam, K. Ahmed, A. Dinovitser, B. W.-H. Ng, and D. Abbott, "Terahertz detection of alcohol using a photonic crystal fiber sensor," Vol. 57, No. 10, 2426–2433, 2018.
24. Van Lanh, C., K. Borzycki, K. D. Xuan, V. T. Quoc, M. Trippenbach, R. Buczyński, and J. Pniewski, "Optimization of optical properties of photonic crystal fibers infiltrated with chloroform for supercontinuum generation," *Laser Physics*, Vol. 29, No. 7, 075107, 2019.

25. Debbal, M., M. Bouregaa, H. Chikh-Bled, M. E. K. Chikh-Bled, and M. C. E. Ouadah, "Influence of temperature on the chromatic dispersion of photonic crystal fiber by infiltrating the air holes with water," *Journal of Optical Communications*, Vol. 1, No. ahead-of-print, 2019.
26. Wang, C., P. P. Shum, D. J. J. Hu, Y.-C. Chen, Z. Xu, S. Liu, Y. Zhang, Y. Zhu, Y. Zheng, and B. Li, "Two-core photonic crystal fiber with selective liquid infiltration in the central air hole for temperature sensing," Vol. 3, No. 8, 2264–2276, 2020.
27. Saitoh, K. and M. Koshiba, "Full-vectorial imaginary-distance beam propagation method based on a finite element scheme: application to photonic crystal fibers," *IEEE Journal of Quantum Electronics*, Vol. 38, No. 7, 927–933, 2002.
28. Habib, M. S., M. S. Rana, M. Moniruzzaman, M. S. Ali, and N. Ahmed, "Highly birefringent broadband-dispersion-compensating photonic crystal fibre over the E+ S+ C+ L+ U wavelength bands," *Optical Fiber Technology*, Vol. 20, No. 5, 527–532, 2014.
29. Huang, T., Q. Wei, Z. Wu, X. Wu, Xu, P. Huang, Z. Cheng, and P. P. Shum, "Ultra-flattened normal dispersion fiber for supercontinuum and dissipative soliton resonance generation at 2 μm," *IEEE Photonics Journal*, Vol. 11, No. 3, 1–11, 2019.
30. Begum, F. and P. E. Abas, "Near infrared supercontinuum generation in silica based photonic crystal fiber," Vol. 89, 149–159, 2019.
31. Upadhyay, A., S. Singh, Y. Prajapati, and R. Tripathi, "Numerical analysis of large negative dispersion and highly birefringent photonic crystal fiber," *Optik*, Vol. 218, 164997, 2020.